

Full length article

Oxygen solutes induced anomalous hardening, toughening and embrittlement in body-centered cubic vanadium

Jian Zhang, Wei-Zhong Han*

Center for Advancing Materials Performance from the Nanoscale, State Key Laboratory for Mechanical Behavior of Materials, Xi'an Jiaotong University, Xi'an 710049, China



ARTICLE INFO

Article history:

Received 25 March 2020

Revised 4 June 2020

Accepted 13 June 2020

Available online 18 June 2020

Keywords:

Vanadium

Oxygen solutes

Hardening

Dislocation debris

Cross-slip

ABSTRACT

Vanadium (V) is sensitive to minute quantity of oxygen interstitials, which induce pronounced hardening and embrittlement. Here, we utilize oxygen to synthesize V solid solutions in order to reveal the mechanism of oxygen solutes induced hardening. With increasing of oxygen solute concentrations, the fracture modes of V samples transform from dimple, to a mixture of dimple and cleavage, and to a fully transgranular cleavage. High density of dislocations and dislocation debris are produced in strained samples. The mobility of screw dislocations is reduced and the dislocation cross-slip events are promoted by oxygen solutes. In addition to oxygen solution hardening, the generation of high density of oxygen-vacancy complexes plays a dominant role in the strengthening. High quantity of loop-shaped dislocation debris are direct evidence for the formation of oxygen-vacancy complexes. Profuse oxygen-vacancy complexes trap dislocations, promote cross-slips and assist dislocation storage, thus give rise to a superior combination of strengthening, strain hardening, and ductility in V with 1.0 at% of oxygen. Once beyond a critical oxygen concentration (>1.6 at%), V shows catastrophic brittle failure due to the exceptional high density of oxygen-vacancy complexes. These findings provide insight to design high performance refractory metals utilizing oxygen solutes.

© 2020 Acta Materialia Inc. Published by Elsevier Ltd. All rights reserved.

1. Introduction

Group VB body-centered-cubic (BCC) metals are widely used in aerospace and nuclear industries because of their corrosion resistance, excellent mechanical properties and radiation tolerance etc. [1–3]. Vanadium (V) and its alloys, for instance, are considered as a potential first-wall/blanket candidate for fusion nuclear reactors owing to their low activation, high thermal conductivity and high-temperature strength [4–10]. However, the development of refractory metals is hindered by an unresolved issue of their high affinity to light elements, including oxygen solutes [11,12]. These undesirable impurities usually come from smelting residue or hot-working process, which induce significant hardening and even embrittlement [13–20].

The strength-ductility trade-off, the increase in the strength with expense of ductility, widely exists in many metals and alloys [21,22]. In general, the mechanical properties mutations by foreign elements are referred as solution hardening [23,24]. The source of strengthening is the elastic interactions between the local stress fields of solute atoms and surrounding dislocations. On one hand,

the dilatational stress by oxygen interstitials increase lattice friction, which make dislocation glide difficult [25–30]. As a result, the yield stress increases while the ductility is impaired with the increasing of oxygen solutes. On the other hand, an attractive force between interstitial solutes and dislocations also induces strengthening and ductility loss [31–37]. However, the plasticity governing mechanism in BCC metals is more complex because of the far intricate behavior of screw dislocations, whose motion is relatively rough due to its three-dimensional core structure [38–40]. Therefore, many efforts are focused on unveiling the behavior of screw dislocations and their effect on the plasticity of BCC metals [41–43]. Recently, a random repulsive force field is revealed in Nb between dispersive oxygen solutes and screw dislocations, which facilitates cross-kinks formation and emit copious vacancies during screw dislocation gliding [44]. Oxygen solutes and vacancies further cluster into oxygen-vacancy complexes owing to their strong binding energy [44]. The trapping of screw dislocations by oxygen-vacancy complexes render remarkable hardening [44]. In addition, oxygen solutes facilitate the stabilization and accumulation of vacancies to produce nano-cavities and to trigger devastating failure [44]. Nevertheless, the three-body interaction of oxygen-vacancy-screw dislocation was proposed largely based on atomistic simu-

* Corresponding author.

E-mail address: wzhanxjtu@mail.xjtu.edu.cn (W.-Z. Han).

lations, further experimental evidences on their interplay mechanism are still lacking.

Based on the mechanism of hardening and embrittlement in BCC metals, several strategies were proposed to avoid the oxygen solutes induced embrittlement and damage, e.g. by alloying or via surface ion implantation [45–47]. However, this suffers from a setback on other inherent properties, for example, alloying reduces melting point and enhances prime cost. Recently, a new strategy is proposed to utilize environmental oxygen to achieve high strength and strain hardening while with little ductility loss in Nb [48]. Besides, some BCC high-entropy alloys, such as TiZrHfNb, the mechanical properties can also be improved by adding oxygen as alloying elements [49]. The extra oxygen solutes form into ordered oxygen complexes with some of the elements, which facilitate dislocation double cross-slips and storage [49]. In regarding to these efforts, it is interesting to explore the mechanism of oxygen solute induced hardening and embrittlement in BCC V.

In this study, we tune the concentration of oxygen solutes in V in order to achieve either strengthening or embrittlement. By adding 1.0 at% of oxygen in V, the yield strength, the strain hardening rate, and the ultimate tensile strength are enhanced simultaneously while the sample still has similar uniform ductility as pure V. However, further catastrophic brittle fracture occurs without any macroscopic plastic deformation even with a slightly enhancing oxygen impurity to 1.7 at%. To unveil the hardening and embrittlement mechanisms associated with the oxygen solutes, we employ both macro- and micro-scale experimental techniques, and focus on the dynamic interactions between dislocations and defect complexes. This study provides direct evidences on the effect of oxygen solutes on dislocation propagation, interaction and storage in V. Different concentration of oxygen solutes in V induces a strength-ductility match, higher strain hardening rate or a devastating failure.

2. Experimental methods

2.1. Preparation of V-oxygen solid solutions

The preparation of V-oxygen (V-O) solid solutions was divided into three steps. Step I, homogenization annealing of hot-rolled polycrystalline V plate (1.0 mm in thickness, 99.95% purity) at 1150°C for 1 hour in a tube furnace with vacuum of 1×10^{-4} Pa. The samples processed by step I are named as pure V. Step II, oxygen charging at high temperature. Pure V was heat-treated in a tube furnace with 20 sccm Ar-5% O₂ (about 250 Pa) during elevating the temperature (10°C/min) to 800°C or 900°C. Then the gas inlet was turned off and the samples were kept for 1 h. The oxygen charged specimens are named as V-O1 and V-O2, respectively. Step III, all V-O specimens were homogenized at 1000°C for 6 hours in high vacuum in order to ensure the homogeneous distribution of oxygen. The average grain size of pure V and V-O samples are all around 100 μm (see the example of pure V in Fig. 1(a)). The initial dislocation density is low ($\sim 10^{13}/\text{m}^2$) due to the fully recrystallization in three types of samples. The concentrations of oxygen, nitrogen, carbon in these samples were measured by LECO ONH836 Oxygen/Nitrogen/Hydrogen Elemental Analyzer and LECO CS844 Carbon/Sulfur Analyzer. X-ray diffraction (XRD, from Bruker) was conducted to exclude possible oxides and new phases in the V-O solid solutions.

2.2. Mechanical tests and microstructure characterization

Bulk tensile samples with dimensions of 12 mm (length) \times 5 mm (width) \times 1 mm (thickness) were cut from the pure V plate by electrical discharge machining, then processed with the methods above. The gauge sections were carefully polished and

Table 1
The composition (at.%) of vanadium specimens with different level of oxygen solutes.

Notation	Element		
	Carbon	Nitrogen	Oxygen
Pure V	0.064	<0.011	0.118
V-O1	0.093	0.016	1.012
V-O2	0.165	0.013	1.668

cleaned before tensile tests. Room-temperature quasi-static tension was performed with a strain rate of $1 \times 10^{-3} \text{ s}^{-1}$ on an MTS tensile machine with an extensometer. More than 3 tests were repeated for each type of sample. Micro-Vickers hardness was measured under a load of 100 gf and holding for 15 s. At least 15 spots were tested on both normal and side surfaces to confirm the homogeneity of tensile samples.

Fracture morphology of pure V and V-O tensile samples was characterized by scanning electron microscope (SEM), while typical deformation microstructures beneath the fracture surface were examined by cutting thin foils using a focused ion beam. To minimize the Ga⁺ damage, final cleaning was performed with a voltage of 5 kV and a current of 47 pA. The dislocation structures were characterized using a JEOL 2100F transmission electron microscope (TEM). TEM thin-foils were prepared by mechanically grinding down to 60 μm in thickness, then followed a twin-jet electropolishing in a solution of 10% perchloric acid + 90% alcohol at a direct voltage of 50 V and -10°C. In-situ mechanical testing was conducted inside 2100F by a TEM electrical tip holder. During in-situ mechanical loading, real-time videos were recorded by a charge-coupled device camera (CCD, Gatan 833) with 10 frames per second.

3. Results

3.1. Oxygen-regulated mechanical properties

To exclude possible contamination during heat treatment, the impurity elements in pure V and V-O solid solutions were measured, as listed in Table 1. Comparing to pure V (~ 0.1 at%), the concentration of oxygen solute in V-O1 and V-O2 raised nearly 10 times (~ 1.0 at%) and 14 times (~ 1.7 at%), respectively. The increasing of carbon concentration is much less than the oxygen, thus the hardening is mainly caused by oxygen solutes. The oxygen concentration in these samples is still lower than the solid solubility of oxygen in V [50]. No oxides are formed according to the XRD patterns of the three samples in Fig. 1(b). A slight shift of diffraction peaks in V-O samples towards lower angle indicates some extent of lattice expansion due to oxygen absorption. The 1.0 at% or 1.7 at% of oxygen solutes induce about 0.13% or 0.24% lattice expansion, respectively. There is a weak fiber texture in the as-annealed pure V, and the texture is reduced slightly after oxygen charging (Fig. 1(b)). In a word, V-O solid solutions were prepared without oxides and other contamination phases.

The true stress-strain responses and work hardening rate (Θ) curves of pure V, V-O1 and V-O2 are shown in Fig. 2(a). Pure V has a yield stress of 186 MPa and a fracture elongation of $\sim 25\%$. After introducing of 1.0 at% oxygen (V-O1), the yield strength increases to 459 MPa, which is almost 2.5 times of pure V. The ultimate tensile strength also increases to 661 MPa (286 MPa in pure V). Besides, V-O1 exhibits a much higher strain hardening rate and a uniform elongation (13.5%) comparable with pure V. In the V-O2 sample (1.7 at% oxygen), however, a sudden failure happens at the very beginning of elastic loading. It has a yield strength of 571 MPa, which is 3.1 times of pure V, however, the total fracture strain is only 0.34% and no apparent strain hardening. Similarly,

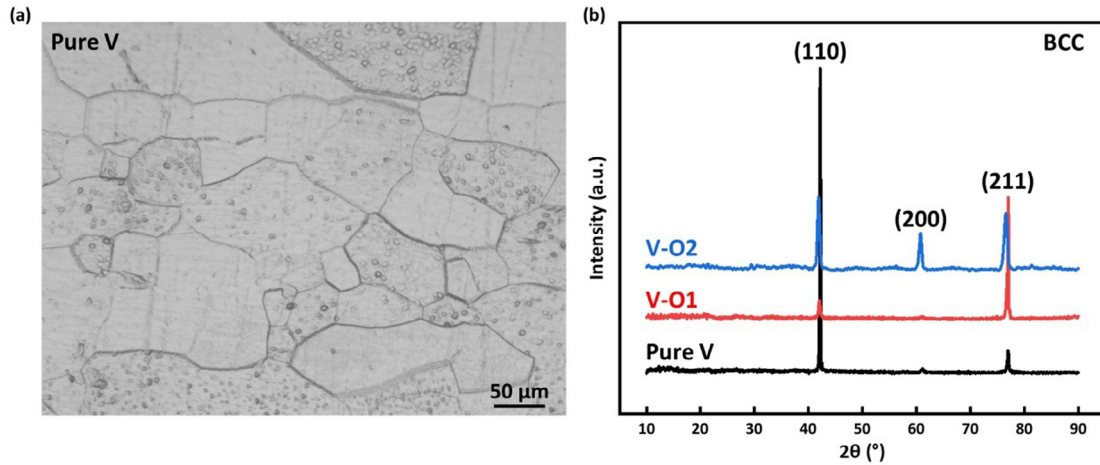


Fig. 1. (a) Initial grain structures in as-annealed pure V; (b) XRD patterns indicate that both pure V and oxygen charged vanadium are body-centered cubic phase. No oxides and other contamination phase are formed.

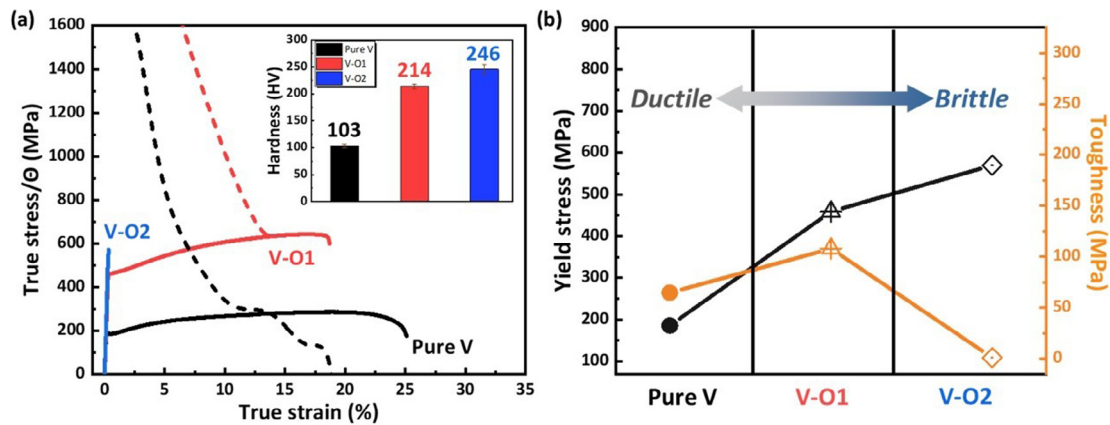


Fig. 2. Tensile properties of bulk pure V and V-O1 and V-O2. (a) Tensile true stress-strain curves and strain hardening rate (Θ) plot (dash lines) of three samples. The insert is the corresponding micro-Vickers hardness. (b) Comparison of yield stress and toughness of three samples. The toughness is the area underneath the true stress-strain curve including necking part.

the hardness (see inset in Fig. 2(a)) also increases with the increasing of oxygen concentrations. Toughness is a critical index for metals, which can be measured by the area under the true stress-strain curves. The variation of toughness and yield strength for the three samples are plotted in Fig. 2(b). Oxygen charging induce a pronounced mechanical property transformation from ductile-to-brittle. Notably, V-O1 has an anomalous combination of high yield strength and toughness, i.e., apparently breaking the envelop of strength-ductility tradeoff.

3.2. Oxygen solutes induced fracture model transition

To gain a better understanding of the effect of oxygen solutes on failure model of V, fracture surfaces were characterized. As shown in Fig. 3(a), the fracture surface is comprised of ridgelines and dimples for pure V, a clear ductile failure. These dimples are ranging from $1 \mu\text{m}$ to $10 \mu\text{m}$ in length. Deformation microstructures underneath the dimples are examined as well. Several ellipsoidal voids in the immediate vicinity of fracture surfaces as well as a micro-cavity approximately $5 \mu\text{m}$ away from the fracture surfaces are captured, as marked in Fig. 3(b). After tensile loading, profuse dislocation cells are formed underneath the fracture sur-

face due to severe plastic deformation in necking (Fig. 3(c)). These cell structures can further evolve into subgrains (Fig. 3(d)). Plastic deformation-induced vacancies cluster into voids and their further coalescences lead to failure [51].

Distinct from the crack mode of pure V, a mixture of both ductile and brittle features form in V-O1 sample (Fig. 4(a)). A ductile necking zone forms at the left part of the fracture surface, as highlighted in Fig. 4(b). The V-O1 sample underwent some extent of necking before quasi-cleavage fracture, which is consistent with the stress drop after passing peak stress in Fig. 2(a). Transgranular cleavage patterns form on the fracture surface, typical cleavage steps and planar fracture traces are highlighted in Fig. 4(c). Underneath the cleavage steps, several sub-micro voids are also produced, as shown in Fig. 4(d). Dense dislocation bands are appeared near the fracture surface along both $\{110\}$ and $\{112\}$ slip planes (Fig. 4(e)). Both voids and profuse dislocations structures in V-O1 indicate that the sample had underwent sufficient plastic deformation before final failure. Although V-O1 sample has a similar uniform ductility as pure V, its final fracture is brittle.

Akin to the V-O1 samples, the V-O2 samples show a complete transgranular fracture (Fig. 5). The fracture surface consists of many sharp edges and rivers, as marked in Fig. 5(b). TEM im-

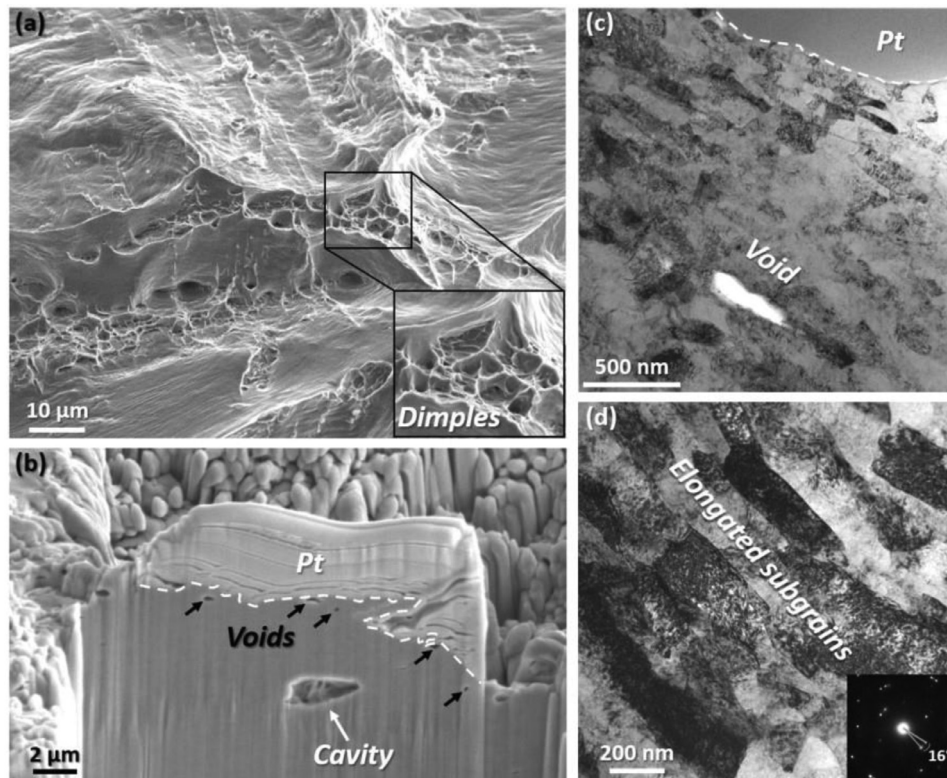


Fig. 3. Ductile fracture morphology of pure V after tensile test. (a) A typical SEM image of fracture surface of pure V containing dimples. (b) Cavities formed beneath a dimple. (c) and (d) Typical TEM images of deformation produced voids and sub-grains beneath a dimple in the front tip. The insert in (d) is the selected area electron diffraction of the sub-grains.

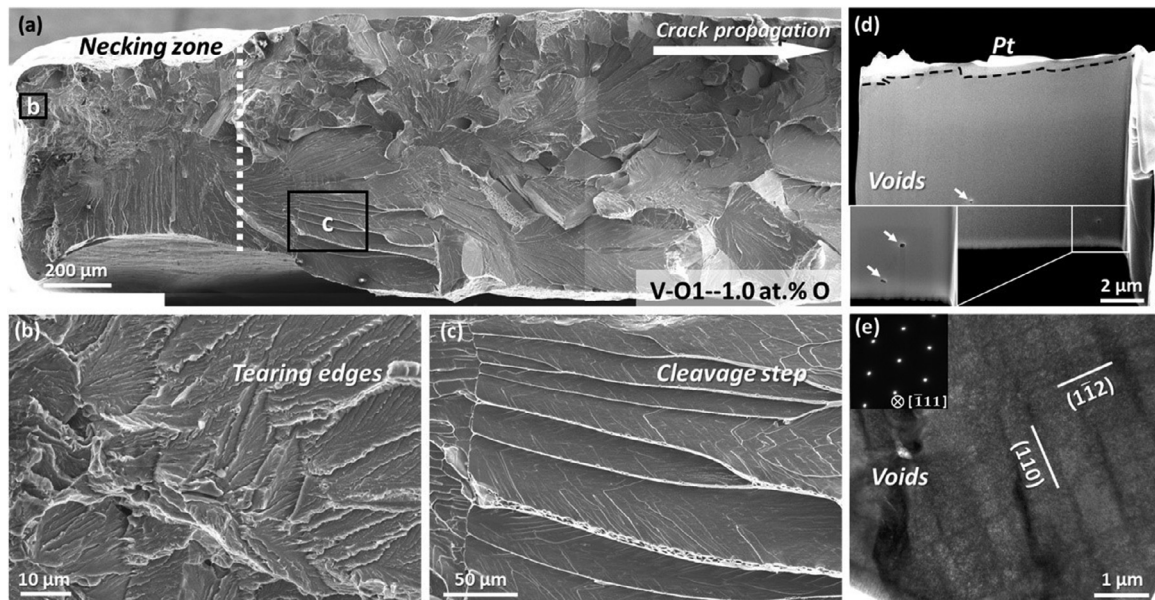


Fig. 4. Fracture surface of V-O1 after tensile test. (a) Overview of the fracture morphology of V-O1. The necking zone indicates some extent of ductile deformation. The right transgranular fracture feature shows a brittle-like failure. The arrow marks the crack propagation direction. (b) An enlarged SEM image in the necking zone displays a quasi-cleavage fracture feature. (c) An enlarged SEM image showing a river pattern. (d) Voids beneath the cleavage steps and (e) is corresponding TEM structure with dislocation bands along $\{110\}$ and $\{112\}$ slip planes.

ages in Fig. 5(c) and (d) show that there are some dislocation activities near fracture surface before the catastrophic failure. While these dislocations are short and straight, and only limit to the region near fracture surface. The dislocation density in this region is $44.5 \mu\text{m}^{-1}$ (number of dislocations in a line vertical to dislocation

with length of 1 micron), indicating a strong localized hardening before fracture, similar to the micro-tensile of Nb single crystals [44]. These observations show that the plastic deformation in V-O2 sample is very limited and only concentrates in the region near fracture surface.

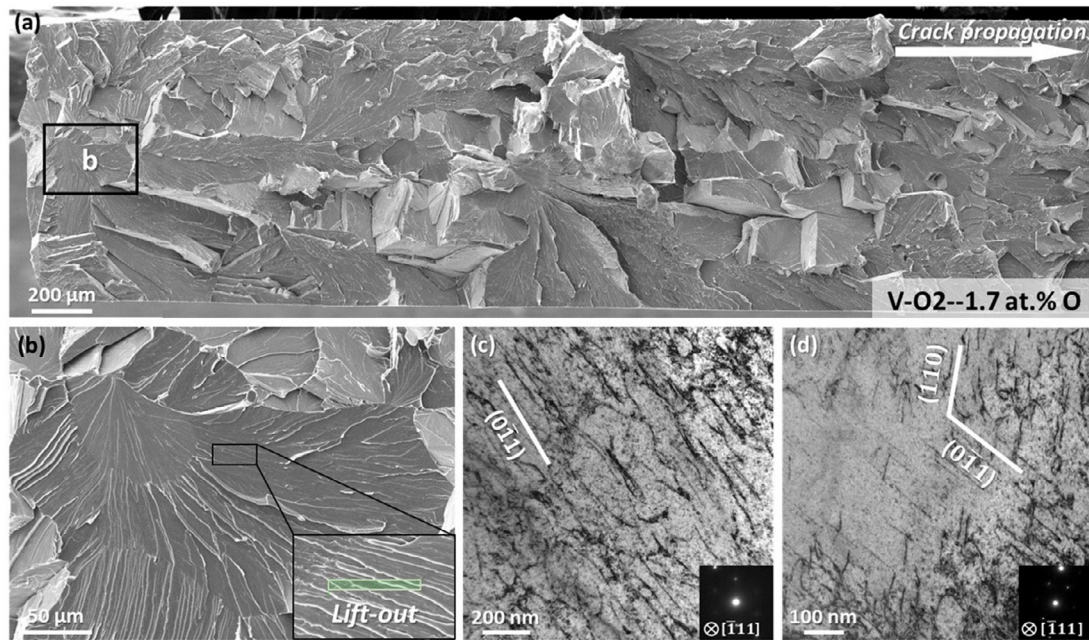


Fig. 5. Fracture surface of V-O2 after tensile test. (a) Overview of the fracture surface of V-O2. The transgranular fracture feature indicate a brittle failure. The arrow marks the direction of crack propagation. (b) An enlarged SEM image showing the near cleavage fracture. The area of river pattern marked in (b) was cut out for further dislocation structures characterization in (c) and (d). TEM images show high density of dislocations aligning along two $\{110\}$ planes.

3.3. Dislocation structures in strained pure V and V-O1

To reveal the complex mechanisms of oxygen solutes induced strengthening and strain hardening, dislocation structures in both pure V and V-O1 at different strain were examined, as shown in Fig. 6. All images were taken with e-beam along $[\bar{1}11]$ and under different two-beam conditions. For pure V, at $\varepsilon = 3\%$, two arrays of dislocations are produced along $\{110\}$ and $\{112\}$ slip planes, as labeled in Fig. 6(b). These dislocations are entangled and form many dislocation junctions and curved segments [52]. They are two sets of long screw dislocations with Burgers vectors of $a/2[11\bar{1}]$ and $a/2[111]$. With increasing the strain to 6%, the entanglement of dislocation becomes more intense. Most dislocation lines are distributed away from the original $\{110\}$ and $\{112\}$ planes and form a complex pattern (Fig. 6(c)). At $\varepsilon = 12\%$, an incipient dislocation network is produced (Fig. 6(d)). High density of dislocations with both long straight lines and curved dislocation network are randomly distributed after fracture (Fig. 6(e)). These observations indicate that the accumulation of dislocations is the main hardening mechanism in pure V.

The evolution of dislocation structures in V-O1 was monitored at similar strains, as marked in Fig. 6(a). At $\varepsilon = 3\%$, some straight dislocation lines are produced (Fig. 6(f)). Curve features on dislocations are signs of dislocation cross-slip or kinks formation. The straight parts are screw dislocations with Burgers vector of $a/2[11\bar{1}]$. Some dislocations show sharp turning points, which is an indication of strong pinning on dislocations. Such local pinning points force dislocations to form a local bowing geometry. When increasing the strain to 7%, the density of straight dislocations increases significantly. Compared to pure V, the dislocations in V-O1 are quite straight and their interaction and entanglement are weaker. Beside the dislocation lines, numerous dislocation debris are produced in the V-O1 sample, as marked in Fig. 6(g). After fracture, profuse long and straight dislocations are well-arranged on $\{110\}$ planes. No curved dislocation networks are formed (Fig. 6(h)), which is distinct from pure V (Fig. 6(e)). Although there are some bowing characters on these long straight screw dislocations, the magnitude of bowing and the curvature is small, indicating a strong and high intensity of pinning, as highlighted in Fig. 6(i). Dis-

location density in the fractured V-O1 ($2.70 \times 10^{14}/\text{m}^2$) is higher than that of pure V ($2.15 \times 10^{14}/\text{m}^2$).

3.4. Effect of oxygen solutes on the dynamic behavior of dislocations

In order to reveal dynamic effect of the oxygen solutes on dislocation behavior, we performed in-situ nanomechanical tests on both the pure V and the V-O1 thin foils, as shown in Fig. 7 and Movie S1 to S2. Upon straining on pure V, dislocations bow out successively from the tip of indenter, as shown in Fig. 7(a) and Movie S1. With the gliding of dislocations, two parallel screw dislocation lines are formed. This observation verifies that the edge dislocations have higher mobility than the screw dislocations [53–55]. Under further straining, the rapid motion of the edge dislocation drags the parallel straight screw parts only extend a little bit, as manifested by the slight curved character in Fig. 7(c). These curved screw dislocations are connected by the half spherical edge part in the top, as shown in Fig. 7(c). These slow-moving screw dislocations lines are primarily on $\{112\}$ planes according to post-mortem characterization in Fig. 7(c) and (d).

In contrast, due to oxygen solutes, the dynamic of dislocations is altered markedly in V-O1, as displayed in Fig. 7(e)–(h) and Movie S2. Upon loading, dislocations also produce in the front of indenter, however, the glide of these dislocations is sluggish (Movie S2), indicating of considerable obstruction on dislocation. Because of the slow gliding of dislocations and continuous emitting of new dislocations in V-O1 sample, a local region with very high dislocation density is formed, as labeled in Fig. 7(e). The character of a singular dislocation in V-O1 is highlighted in Fig. 7(f). Notably, a large number of dislocations start to cross-slip at the tip region of indenter, as marked in Fig. 7(e) and Movie S2. The cross-slip produces high density of parallel dislocation lines after straining (Fig. 7(g) and (h)). These parallel screw dislocation lines have a density of about $38.7 \mu\text{m}^{-1}$, which is two times of the dislocations in strained pure V ($17.3 \mu\text{m}^{-1}$). The extra high density of dislocations in strained V-O1 indicates that the oxygen solutes can suppress dislocation annihilation and significantly enhance dislocation storage.

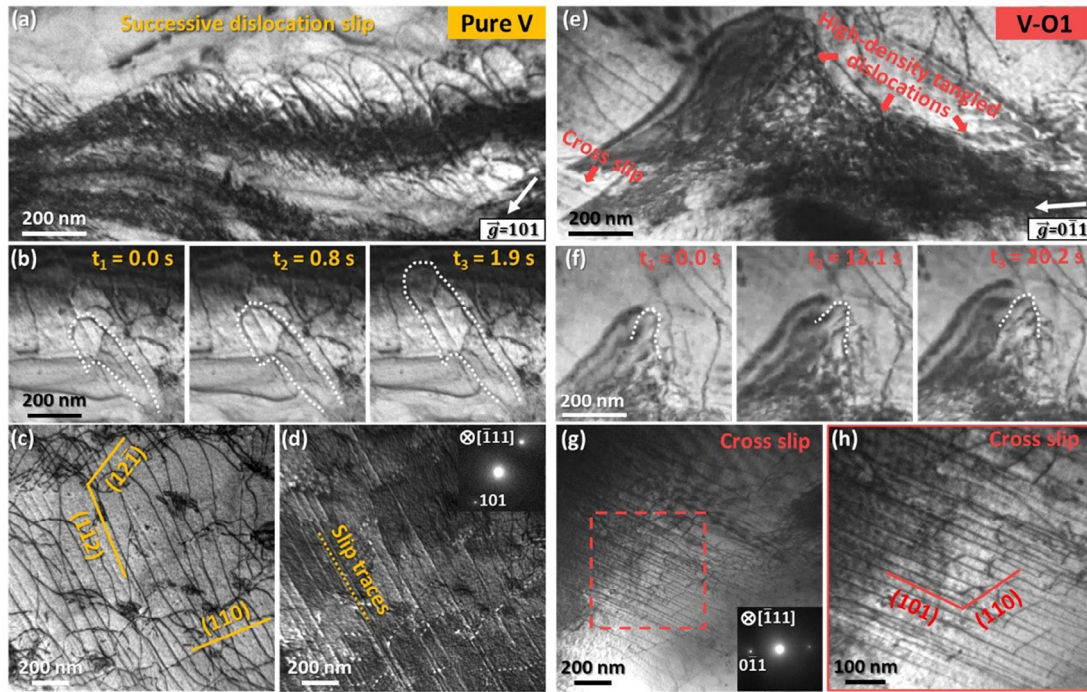


Fig. 7. In-situ compression tests taken along $[\bar{1}11]$ beam direction showing the dynamics of dislocations in pure V ((a)-(d)) and V-O1 ((e)-(h)). (a) and (e) show bowing out of dislocations under in-situ loading. (b) and (f) highlight the individual dislocations. (c), (d) and (g) Dislocation structures produced after indentation. (h) is an enlarged image of area marked in (g).

where $\mu = 47$ GPa is the shear modulus. Yang et al. [44] reported that there is a weak binding energy (~ 0.2 eV) between edge dislocation and oxygen solute in Nb. Because of VB group BCC metals have similar electronic configuration and crystal structure, we adopt this value here to calculate solution hardening in oxygen charged V. The magnitude of f_0 is estimated as $\Delta E/b = 0.2$ eV/0.26 nm = 0.12 nN. Γ is about 1.6 nN. c_0 on (110) slip plane is estimated as $c/(a \times \sqrt{2}a)$, where c is the concentration of oxygen in Table 1 and a is the lattice constant. Thus, σ_{ss} is 24 MPa for pure V. According to the yield stress in Fig. 2(a), the total hardening by Peierls stress and impurity (σ_1) is 162 MPa, as plotted in Fig. 8. This value is used as a constant to estimate the strengthening in oxygen charged V. According to Eq. (2), oxygen solution hardening in V-O1 and V-O2 are 76 MPa and 99 MPa, as plotted in Fig. 8(a). Notably, the measured yield stresses in both oxygen-charged V samples are higher than the sum of hardening by Peierls stress, impurity and oxygen solutes, as shown in Fig. 8(a). This discrepancy indicates that there is addition hardening component which is not involved in the current model. Nevertheless, an exceptional combination of strength, ductility and strain hardening is achieved in V-O1 (Fig. 2), which requires a more reasonable explanation.

In an earlier study, a repulsive interaction is observed between oxygen solutes and screw dislocation in Nb [44]. However, a strong three body interaction among oxygen solute, vacancy and screw dislocation is captured [44]. Screw dislocations moving through the dispersed oxygen-vacancy complexes are pinned and require more stress to break free [44,48]. This is a common phenomenon for VB transition BCC metals according to the first-principles calculations [44]. The interaction between oxygen atom and screw dislocation is also repulsive (1 eV) in V, thus oxygen solutes cannot directly lock screw dislocations. However, vacancies in V can trap oxygen solutes to form stable configuration of complexes with the binding energy in the range of 0.4 ~ 0.8 eV [59–62]. Therefore, similar to that in Nb [44], oxygen-vacancy complexes can obstruct the motion of screw dislocation in V, which should be the missed hardening component. During oxygen charging at high temperature,

profuse oxygen-vacancy complexes are supposed to be produced through the combination of thermally excited vacancies and diffuse in oxygen solutes, which lock mobile dislocations and enhance the yield strength of both V-O1 and V-O2 samples. Therefore, the yield strength in oxygen charged V should include three contributions, the Peierls stress and impurity hardening, the oxygen solution hardening and the oxygen-vacancy complexes hardening.

4.2. Oxygen-vacancy complexes induced dynamic hardening in V

For V-O1, simultaneous increase in yield stress, strain hardening, ultimate tensile stress and uniform elongation are observed (Fig. 2). In general, the strain hardening in metal is induced by the dynamic accumulation of dislocations. The dislocation density in both failed pure V and V-O1 have been measured, thus the amount of stress increase after yielding can be estimated according to Taylor equation ($\sigma_{dis} = M\alpha_{dis}\mu b\sqrt{\rho_{dis}}$, $\alpha_{dis}=0.22$) [63], as plotted in Fig. 8(b). By adding the hardening induced by dislocation accumulation in V-O1, the calculated flow stress is still lower than the experimental value, while this simple model works for pure V. The discrepancy indicates that there is a missing strain hardening component.

In the earlier study in oxygen-charged Nb, a strong strain hardening is observed due to the dynamically formation of oxygen-vacancy complexes [44]. Due to the strong repulsive interaction between screw dislocations and oxygen interstitials, a random force field emerges, which results in successive cross-kink formation and pinching off during screw dislocation motion at moderate strain rate. This pinching off process generates profuse point defects including vacancies and self-interstitials. Thus profuse oxygen-vacancy complexes are formed due to their strong binding energy. These oxygen-vacancy complexes have strong attractive interaction with screw dislocation thus trap dislocations and induce a significant strain hardening. Interestingly, oxygen-vacancy complexes are stable even after successive dislocations sweeping in contrast to the unstable vacancies and self-interstitials [44]. Limited by the de-

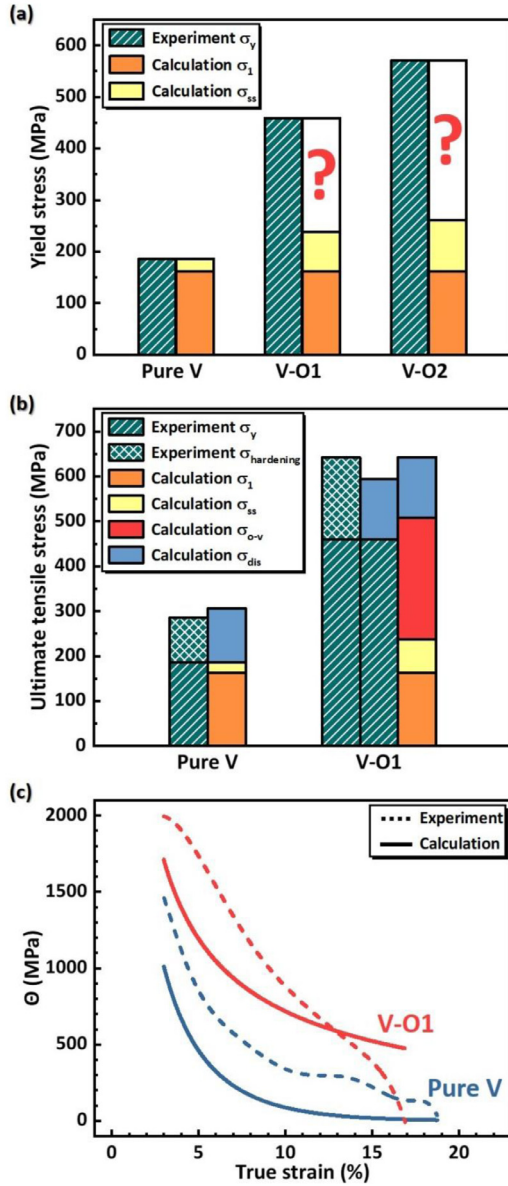


Fig. 8. (a) Model prediction of the yield strength of pure V, V-O1 and V-O2 samples. (b) Model prediction of the ultimate tensile strength of pure V, V-O1 and V-O2 samples. (c) Comparison of strain hardening curves of experiments and estimations according to the dynamic precipitation of oxygen-vacancy complexes.

tection ability of experimental instruments, such atomic-scale defects and their interaction are discovered based on atomistic simulations [44]. Direct experimental validation of such a novel mechanism is very challenging.

Similar to Nb, dynamical formation of oxygen-vacancy complexes also plays an important role in deformation of V-O1. Although the oxygen-vacancy complexes are invisible under normal TEM condition, there should be some products after dislocations passing through them, similar to the Orowan loop left on the precipitates [64,65]. As mentioned in Section 3, in addition to the high density of line dislocations, a large quantity of diversely distributed small elliptical dislocation debris have been observed after a certain amount of deformation, as shown in Figs. 6 and 9. These dislocation debris appear only in the form of unresolvable spots with the average size of a few nm, and widely detected in both strained pure V and V-O1 (Fig. 6(i) and Fig. 9). Therefore, the loop-shaped dislocation debris are Orowan loops, which are

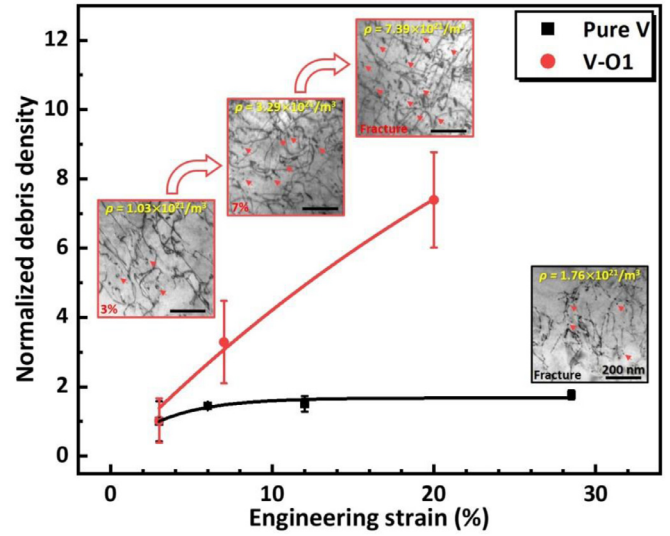


Fig. 9. Evolution of the number density of dislocation debris during tensile deformation of pure V and V-O1 samples. The density of dislocation debris is normalized by taking the debris density in pure V at 3% strain as one. The exponential fitting shows the evolution of debris density with strain. Oxygen solutes promote the production of dislocation debris, which are Orowan loops and is the reflection of the formation of oxygen-vacancy complexes. The scale bars are 200 nm.

likely the developer of the interaction between dislocations and oxygen-vacancy complexes. In order to monitor the evolution of such debris with strain, we measured the density of dislocation debris and plotted in Fig. 9. A striking difference is appeared for pure V and V-O1. After yielding, the debris density in pure V is about $1.00 \times 10^{21}/m^3$ and only slightly increases to approximate $1.76 \times 10^{21}/m^3$ before failure. In contrast, the density of dislocation debris increases markedly with plastic strain in V-O1. After 3% strain, the number of debris in V-O1 is similar to that in pure V. While a 7 times increase in the number density of debris in V-O1 after fracture, such as $7.39 \times 10^{21}/m^3$. This value is only an underestimation because some of oxygen-vacancy complexes are likely not decorated by dislocation segments yet. The significant increasing of the number density of oxygen-vacancy complexes and their interaction with dislocations are the dominant mechanism for remarkable strain hardening in V-O1.

According to these observations, the stress increment σ_{o-v} due to the dynamic formation of oxygen-vacancy complexes can be expressed by a modified Orowan equation [64–66]:

$$\sigma_{o-v} = M\tau_{o-v} = M \frac{\alpha \mu b}{2\pi \sqrt{1-\nu} \lambda} \ln\left(\frac{r}{b}\right) \quad (3)$$

where α is an average value of the pinning site strength, and is about 0.85 for impenetrable particles [66,67]; r is the average radius of loop-shaped debris (2.4 nm); λ is the average spacing between oxygen-vacancy complexes, which is not a constant and gradually decrease with increasing of plastic strain. λ is proportional to $1/\sqrt{\rho_{debris}}$, where ρ_{debris} is the density of dislocation debris in Fig. 9. According to Fig. 9, the variation of debris density with strain can be obtained by exponential fitting. Based on these relations, the strain hardening rate ($\Theta = d\sigma/d\varepsilon$) of pure V and V-O1 due to the dynamic formation of oxygen-vacancy complexes can be calculated, as plotted in Fig. 8(c). In general, the model captures the trend of experimentally measured strain hardening rate for V-O1, indicating that the dynamic production of oxygen-vacancy complexes is the dominant strain hardening mechanism. Notably, the contribution of oxygen-vacancy complexes on total hardening rate continuously increase with the strain (Fig. 8(c)). The lower strain hardening rate in comparison to experiment is

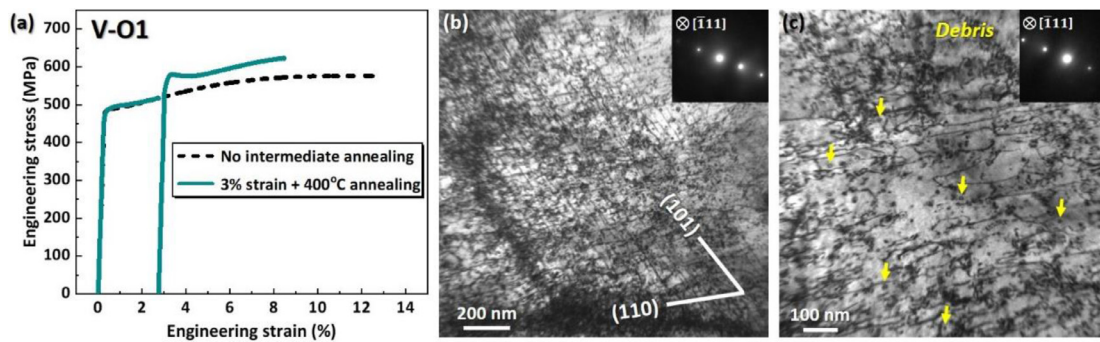


Fig. 10. (a) Tensile stress-strain curves of V-O1 samples with and without intermediate annealing. (b) and (c) Defects structures in failed V-O1 sample with intermediate annealing. Extremely high density of screw dislocations and loop-shaped dislocation debris are produced.

because of additional hardening by the storage of dislocations. In contrast, the oxygen-vacancy induced strain hardening in pure V is much lower than the experimental strain hardening rate (Fig. 8(c)), displaying that the formation of oxygen-vacancy complexes is not the dominant hardening mechanism, whereas the accumulation of dislocations leads to the strain hardening. The total hardening in V-O1 is plotted in Fig. 8(b), which including Peierls stress and impurity hardening, oxygen solutes hardening, oxygen-vacancy complexes hardening and dislocation storage hardening.

The dynamic formation of oxygen-vacancy complexes requires transportation of oxygen solutes or vacancies during straining. Atomistic simulations show that screw dislocation can sweep away oxygen solutes or transport vacancies via a displacive mechanism at ambient temperature [44], while such mechanism is less efficient than the thermal annealing. In order to further justify that the formation of oxygen-vacancy complexes is the dominant hardening mechanism, we performed an intermediate annealing tensile test in order to accelerate the formation of oxygen-vacancy complexes, as shown in Fig. 10. After 3% tensile strain, the V-O1 was annealed at 400°C for 1 h, then continue pulled under a similar condition. Comparing to the normal stress-strain curve of V-O1, the intermediate-annealed sample shows a near 91 MPa increase in flow stress, then follows a steep strain hardening and fractured. The final fracture stress is much higher than that of V-O1. This behavior is related to the annealing-assisted precipitation of oxygen-vacancy complexes. The microstructures in failed sample are shown in Fig. 10(b) and (c). Extremely high density of screw dislocations ($3.01 \times 10^{14}/\text{m}^2$) and loop-shaped debris ($9.15 \times 10^{21}/\text{m}^3$) are remained in the sample, indicating either annealing or straining promote the formation of oxygen-vacancy complexes, which is the dominant hardening mechanism. Similar phenomenon is also observed in oxygen alloyed Nb [37].

4.3. Synergy effect of oxygen solutes on strength, ductility and embrittlement

The impurity elements doping strategy can improve the strength markedly, while a sacrifice in ductility always arise. In general, the cause of brittle is due to the completely locking of mobile dislocations by formation of oxygen-vacancy complexes. For V-O2, assuming the additional increasing in yield stress are all related to the oxygen-vacancy complexes, such as 311 MPa for V-O2, the estimated number density of oxygen-vacancy complexes in the as-received samples is as high as $1.12 \times 10^{22}/\text{m}^3$. Due to the extremely high density of oxygen-vacancy complexes, the dislocations almost cannot glide. Although the yield strength is tripled

(this is likely an underestimation due to stress concentration induced premature failure), it shows a totally brittle fracture with zero macroscopic plasticity in V-O2. Actually, there are some dislocation activities in the adjacent of crack (Fig. 5(c) and (d)) due to stress concentration. Such localized deformation provides sufficient point-defects like vacancies. These dispersed oxygen solutes not only combine with vacancies to pin screw dislocations, but also can collect additional vacancies to produce nano-cavities [44]. Limited by the time resolution of nano-cavities forming, it is difficult to capture the damage process under normal experimental condition. Atomistic simulations had shown that these nano-cavities grew out of the oxygen-vacancy complexes [44]. With continuous screw dislocations passing, a long hollow oxygen-vacancy tube gradual takes shape as oxygen-vacancy complexes forming [44]. This oxygen-vacancy tube is quite stable from collapsing because of the relative high content of dispersed oxygen atoms along the tube. Later screw dislocations continue the same action along the existing vacancy tube. With more and more oxygen-vacancy tubes form near each other, these nano-cavities would eventually coalesce and result in crack initiation in an expected prolate-to-oblate transition, a process driven by elasticity. As a result, the oxygen-vacancy tube grows into detectable nano-cracks. The nano-crack can further grow and coalesce to induce semi-cleavage fracture. The observation of nano-cavities underneath the fracture surface support such a picture of damage (Figs. 3 to 4).

However, for the sample with mediate range of oxygen, such as 1.0 at% oxygen solutes, the yield stress is increased markedly (2.5 times of pure V), but the uniform elongation remains unchanged due to the remarkable strain hardening ability (Fig. 2). As discussed in 4.2, the excellent strain hardening in V-O1 comes from the dynamic formation of oxygen-vacancy complexes, which continuously lock dislocations. The density of oxygen-vacancy complexes (measured by dislocation debris) increases remarkably with strain (Fig. 9), thus dislocation slip becomes harder and harder. In order to continue deformation, dislocations start to cross-slip (Fig. 7), this promotes the accumulation and multiplication of more dislocations. All of such processes contribute to the strain hardening. The 1.0 at% oxygen interstitials have the combined effect of pinning and storage of dislocations (Fig. 6(f) to (h)). The bowing-out geometry of dislocations and ever-growing dislocation debris are the reflection of the interaction between dislocations and oxygen-vacancy complexes (Figs. 6 and 8). Dynamic precipitation of oxygen-vacancy complexes and dislocation cross-slip are two key mechanisms in enhancing the tensile ductility and toughness. As a result, appropriate solutes tuning is capable to design an oxygen solution with an exceptional synergy of strength, strain hardening and ductility.

5. Conclusions

In this study, the influence of oxygen solute concentrations on the plastic deformation of V are investigated. Main findings are as follows:

- (1) The mechanical response under room temperature tensile demonstrates a strong oxygen solutes sensitivity in V. Pure V shows ductile deformation with dimples on fracture surface. V-O1 (1.0 at% oxygen) displays enhanced strength, hardness and strain hardening rate and without loss in ductility. A mixture of ductile and brittle features coexists on the fracture surface. V-O2 (1.7 at% oxygen) demonstrates devastating brittle failure with zero macroscopic plastic strain and completely transgranular cleavage.
- (2) Dislocations in the strained V-O1 sample have many pinning sites and display bow-out characters. Screw dislocations are dominant due to the strong interaction with oxygen-vacancy complexes, thus reached a much higher density compared to the strained pure V. In addition to straight dislocation lines, extremely high density of loop-shaped dislocation debris is produced in the deformed V-O1, which is a direct evidence for the dynamic formation of oxygen-vacancy complexes.
- (3) In addition to the solid solution strengthening, the annealing-promoted or the strain-triggered formation of oxygen-vacancy complexes are the dominant mechanism for the anomalous yield strength and strain hardening increase. Once the density of oxygen-vacancy complexes reaches a critical value, such as $7.39 \times 10^{21}/\text{m}^3$, a complete embrittlement of V is appeared. Therefore, it is possible to tune the concentration of oxygen solutes to design refractory metals with good combination of high strength and high ductility.

Declaration of Competing Interest

The authors declare that there are no competing interests.

Acknowledgments

This research was supported by the National Natural Science Foundation of China (Grant Nos. 51922082, 51971170 and 51942104), the National Key Research and Development Program of China (2017YFB0702301), the 111 Project of China (Grant Number BP2018008) and the Innovation Project of Shaanxi Province (Grant No. 2017KTPT-12). J.Z. appreciates the assistance of Dr. P.J. Yang during the earlier stage of this project.

Supplementary materials

Supplementary material associated with this article can be found, in the online version, at doi:[10.1016/j.actamat.2020.06.023](https://doi.org/10.1016/j.actamat.2020.06.023).

References

- [1] J.T. Busby, K.J. Leonard, Space fission reactor structural materials: Choices past, present, and future, *J. Occup. Med.* 59 (2007) 20–26.
- [2] M.S. El-Genk, J.M. Tournier, A review of refractory metal alloys and mechanically alloyed-oxide dispersion strengthened steels for space nuclear power systems, *J. Nucl. Mater.* 340 (2005) 93–112.
- [3] H. Matsui, K. Fukumoto, D.L. Smith, H.M. Chung, W.V. Witzenburg, S.N. Votnov, Status of vanadium alloys for fusion reactors, *J. Nucl. Mater.* 233–237 (1996) 92–99.
- [4] T. Muroga, Vanadium for nuclear systems, In: R.J.M. Konings (Ed.), *Compr. Nucl. Mater.* Elsevier, Amsterdam (2012) 391–406.
- [5] T. Muroga, J.M. Chen, V.M. Chernov, R.J. Kurtz, M. Le Flem, Present status of vanadium alloys for fusion applications, *J. Nucl. Mater.* 455 (2014) 263–268.
- [6] D.L. Smith, M.C. Billone, K. Natesan, Vanadium-base alloys for fusion first-wall/blanket applications, *Int. J. Refract. Metals Hard Mater.* 18 (2000) 213–224.
- [7] D.L. Smith, B.A. Loomis, D.R. Diercks, Vanadium-base alloys for fusion reactor applications – a review, *J. Nucl. Mater.* 135 (1985) 125–139.
- [8] K. Ehrlich, Materials research towards a fusion reactor, *Fusion Eng. Des.* 56–57 (2001) 71–82.
- [9] H.M. Chung, B.A. Loomis, D.L. Smith, Properties of vanadium-base alloys irradiated in the Dynamic Helium Charging Experiment, *J. Nucl. Mater.* 233–237 (1996) 466–475.
- [10] R.J. Kurtz, K. Abe, V.M. Chernov, D.T. Hoelzer, H. Matsui, T. Muroga, G.R. Odette, Recent progress on development of vanadium alloys for fusion, *J. Nucl. Mater.* 329–333 (2004) 47–55.
- [11] R.C. Svedberg, R.W. Buckman, Gas-metal reactions in vanadium and vanadium-base alloys, *Int. Metals Rev.* 25 (1980) 223–231.
- [12] J. Wadsworth, T.G. Nieh, J.J. Stephens, Recent advances in aerospace refractory metal alloys, *Int. Mater. Rev.* 33 (1988) 131–150.
- [13] R.J. Kurtz, Effect of oxygen on the crack growth behavior of V-4Cr-4Ti at 600°C, *J. Nucl. Mater.* 283–287 (2000) 822–826.
- [14] O.N. Carlson, D.G. Alexander, G. Elsnor, The effect of oxygen on the strength and ductility of polycrystalline vanadium in the range of 4.2 to 400 K, *Metall. Trans. A* 8 (1977) 99–104.
- [15] K. Natesan, W.K. Soppet, M. Uz, Effects of oxygen and oxidation on tensile behavior of V-4Cr-4Ti alloy, *J. Nucl. Mater.* 258–263 (1997) 1476–1481.
- [16] J. Chen, S. Qiu, L. Yang, Z. Xu, Y. Deng, Y. Xu, Effects of oxygen, hydrogen and neutron irradiation on the mechanical properties of several vanadium alloys, *J. Nucl. Mater.* 302 (2002) 135–142.
- [17] M. Koyama, K. Fukumoto, H. Matsui, Effects of purity on high temperature mechanical properties of vanadium alloys, *J. Nucl. Mater.* 329–333 (2004) 442–446.
- [18] B.A. Pint, J.R. Distefano, The role of oxygen uptake and scale formation on the embrittlement of vanadium alloys, *Oxid. Metals* 63 (2005) 33–55.
- [19] J.R. DiStefano, J.H. DeVan, Reactions of oxygen with V-Cr-Ti alloys, *J. Nucl. Mater.* 249 (1997) 150–158.
- [20] T. Nagasaka, T. Muroga, K. Fukumoto, H. Watanabe, M.L. Grossbeck, J. Chen, Development of fabrication technology for low activation vanadium alloys as fusion blanket structural materials, *Nucl. Fusion* 46 (2006) 618–625.
- [21] R.O. Ritchie, The conflicts between strength and toughness, *Nat. Mater.* 10 (2011) 817–822.
- [22] E. Ma, T. Zhu, Towards strength–ductility synergy through the design of heterogeneous nanostructures in metals, *Mater. Today* 20 (2017) 323–331.
- [23] Y. Nakada, A.S. Keh, Solid solution strengthening in Fe-N single crystals, *Acta Metall.* 16 (1968) 903–914.
- [24] S. Schmauder, C. Kohler, Atomistic simulations of solid solution strengthening of α -iron, *Comput. Mater. Sci.* 50 (2011) 1238–1243.
- [25] R.H. Li, P.B. Zhang, X.Q. Li, C. Zhang, J.J. Zhao, First-principles study of the behavior of O, N and C impurities in vanadium solids, *J. Nucl. Mater.* 435 (2013) 71–76.
- [26] L.J. Gui, Y.L. Liu, First-principles studying the properties of oxygen in vanadium: Thermodynamics and tensile/shear behavior, *Comput. Condens. Matter* 7 (2016) 7–13.
- [27] M.G. Jo, P.P. Madakashira, J.Y. Suh, H.N. Han, Effect of oxygen and nitrogen on microstructure and mechanical properties of vanadium, *Mater. Sci. Eng. A* 675 (2016) 92–98.
- [28] T. Kainuma, N. Iwao, T. Suzuki, R. Watanabe, Effects of oxygen, nitrogen and carbon additions on the mechanical properties of vanadium and V/Mo alloys, *J. Nucl. Mater.* 80 (1979) 339–347.
- [29] D.L. Harrod, R.E. Gold, Mechanical properties of vanadium and vanadium-base alloys, *Int. Metals Rev.* 25 (1980) 163–222.
- [30] E.A. Loria, Some aspects of vanadium metallurgy in reference to nuclear reactor applications, *J. Nucl. Mater.* 61 (1976) 158–168.
- [31] D. Rodney, L. Ventelon, E. Clouet, L. Pizzagalli, F. Willaime, Ab initio modeling of dislocation core properties in metals and semiconductors, *Acta Mater.* 124 (2017) 633–659.
- [32] M. Kuzmina, M. Herbig, D. Ponge, S. Sandlobes, D. Raabe, Linear complexes: Confined chemical and structural states at dislocations, *Science* 349 (2015) 1080–1083.
- [33] B.A. Bilby, On the interactions of dislocations and solute atoms, *Proc. Phys. Soc. A* 63 (1950) 191–200.
- [34] Q. Yu, L. Qi, T. Tsuru, R. Traylor, D. Rugg, J.W. M. Jr, M. Asta, D.C. Chrzan, A.M. Minor, Origin of dramatic oxygen solute strengthening effect in titanium, *Science* 347 (2015) 635–639.
- [35] N.I. Medvedeva, Y.N. Gornostyrev, A.J. Freeman, Solid solution softening and hardening in the group-V and group-VI bcc transition metals alloys: First principles calculations and atomistic modeling, *Phys. Rev. B* 76 (2007) 212104.
- [36] K. Lu, L. Lu, S. Suresh, Strengthening materials by engineering coherent internal boundaries at the nanoscale, *Science* 324 (2009) 349–352.
- [37] E. Miura, K. Yoshimi, S. Hanada, Oxygen–molybdenum interaction with dislocations in Nb–Mo single crystals at elevated temperatures, *Acta Mater.* 50 (2002) 2905–2916.
- [38] V. Vitek, V. Paidar, Non-planar dislocation cores: A ubiquitous phenomenon affecting mechanical properties of crystalline materials, In: J.P. Hirth (Ed.), *Dislocations in Solids*, Elsevier, Amsterdam, (2008) 439–514.
- [39] J.R. Greer, J.T.M.D. Hosson, Plasticity in small-sized metallic systems: Intrinsic versus extrinsic size effect, *Prog. Mater. Sci.* 56 (2011) 654–724.
- [40] A. Argon, *Strengthening Mechanisms in Crystal Plasticity*, Oxford University Press, New York, 2008.
- [41] J.W. Christian, Some surprising features of the plastic deformation of body-centered cubic metals and alloys, *Metall. Trans. A* 14 (1983) 1237–1256.

- [42] M. Tang, L.P. Kubin, G.R. Canova, Dislocation mobility and the mechanical response of b.c.c. single crystals: A mesoscopic approach, *Acta Mater.* 46 (1998) 3221–3235.
- [43] D. Caillard, Kinetics of dislocations in pure Fe. Part II. In situ straining experiments at low temperature, *Acta Mater.* 58 (2010) 3504–3515.
- [44] P.J. Yang, Q.J. Li, T. Tsuru, S. Ogata, J.W. Zhang, H.W. Sheng, Z.W. Shan, G. Sha, W.Z. Han, J. Li, E. Ma, Mechanism of hardening and damage initiation in oxygen embrittlement of body-centred-cubic niobium, *Acta Mater.* 168 (2019) 331–342.
- [45] T. Nagasaka, T. Muroga, K. Fukumoto, H. Watanabe, M.L. Grossbeck, J. Chen, Development of fabrication technology for low activation vanadium alloys as fusion blanket structural materials, *Nucl. Fusion* 46 (2006) 618–625.
- [46] T. Nagasaka, T. Muroga, H. Watanabe, R. Kasada, N. Iwata, A. Kimura, Mechanical properties of V–4Cr–4Ti alloy after first-wall coating with tungsten, *J. Nucl. Mater.* 417 (2011) 306–309.
- [47] P.J. Yang, W.Z. Han, Enhanced oxidation resistance in refractory niobium by surface Ti+/Si+ implantation, *Corros. Sci.* 163 (2020) 108297.
- [48] P.J. Yang, Q.J. Li, W.Z. Han, J. Li, E. Ma, Designing solid solution hardening to retain uniform ductility while quadrupling yield strength, *Acta Mater.* 179 (2019) 107–118.
- [49] Z. Lei, X. Liu, Y. Wu, H. Wang, S. Jiang, S. Wang, X. Hui, Y. Wu, B. Gault, P. Kontis, D. Raabe, L. Gu, Q. Zhang, H. Chen, H. Wang, J. Liu, K. An, Q. Zeng, T.G. Nieh, Z. Lu, Enhanced strength and ductility in a high-entropy alloy via ordered oxygen complexes, *Nature* 563 (2018) 546–550.
- [50] H.A. Wriedt, The O–V (Oxygen–Vanadium) system, *Bull. Alloy Phase Diagr.* 10 (1989) 271–277.
- [51] B.L. Boyce, B.G. Clark, P. Lu, J.D. Carroll, C.R. Weinberger, The morphology of tensile failure in tantalum, *Metall. Mater. Trans. A* 44 (2013) 4567–4580.
- [52] V.V. Bulatov, L.L. Hsiung, M. Tang, A. Arsenlis, M.C. Bartelt, W. Cai, J.N. Florando, M. Hiratani, M. Rhee, G. Hommes, T.G. Pierce, T. Diaz de la Rubia, Dislocation multi-junctions and strain hardening, *Nature* 440 (2006) 1174–1178.
- [53] D. Caillard, Kinetics of dislocations in pure Fe. Part I. In situ straining experiments at room temperature, *Acta Mater.* 58 (2010) 3493–3503.
- [54] C. Woodward, S.I. Rao, Ab-initio simulation of isolated screw dislocations in bcc Mo and Ta, *Philos. Mag. A* 81 (2001) 1305–1316.
- [55] F.R. Nabarro, M.S. Duesbery, *Dislocations in Solids*, (2nd ed.), North-Holland, Amsterdam (1989).
- [56] R. Labusch, A statistical theory of solid solution hardening, *Phys. Status Solidi.* 41 (1970) 659–669.
- [57] F.R. Nabarro, The theory of solution hardening, *Philos. Mag.* 35 (1977) 613–622.
- [58] R.L. Fleischer, Rapid solution hardening, dislocation mobility, and the flow stress of crystals, *J. Appl. Phys.* 33 (1962) 3504–3508.
- [59] S.C. Agarwal, D.I. Potter, A. Taylor, Effects of oxygen addition on the void-swelling behavior of vanadium, *Metall. Trans. A* 9 (1978) 569–576.
- [60] T.T. Zou, P.B. Zhang, J.J. Zhao, P.F. Zheng, J.M. Chen, First principles study of vacancy-solute complexes in vanadium, *J. Alloys Compd* 73 (2018) 861–866.
- [61] X.M. Zhang, Y.F. Li, Q.L. He, R.L. Li, L. Deng, L. Wang, X.L. Liu, J.F. Tang, H.Q. Deng, W.Y. Hu, Investigation of the interstitial oxygen behaviors in vanadium alloy: A first-principles study, *Curr. Appl. Phys.* 18 (2018) 183–190.
- [62] A.V. Veen, H. Eleveld, M. Clement, Helium impurity interactions in vanadium and niobium, *J. Nucl. Mater.* 212–215 (1994) 287–292.
- [63] G.I. Taylor, The mechanism of plastic deformation of crystals, *Proc. R. Soc. A* 145 (1934) 362–387.
- [64] L.M. Brown, R.K. Ham, Dislocation-particle interactions, in: A Kelly, R.B. Nicholson (Eds.), *Strengthening Methods in Crystals*, Appl. Sci. Publ., London, 1971, pp. 9–135.
- [65] W.Z. Han, A. Vinogradov, C.R. Hutchinson, On the reversibility of dislocation slip during cyclic deformation of Al alloys containing shear-resistant particles, *Acta Mater.* 59 (2011) 3720–3736.
- [66] B.C. De Cooman, Y. Estrin, S.K. Kim, Twinning-induced plasticity (TWIP) steels, *Acta Mater.* 142 (2018) 283–362.
- [67] J.G. Sevillano, Flow stress and work hardening, in: H. Mughrabi, R.W. Cahn, P. Hassen, E.J. Kramer (Eds.), *Materials Science and Technology: A Comprehensive Treatment*, Wiley-VCH, Weinheim, 2006, pp. 10–88.